

## 18. WIND-TUNNEL STUDIES OF NACELLE INTERFERENCE DRAG

### AT HIGH SUBSONIC SPEEDS INCLUDING

#### THE EFFECT OF POWERED JETS

By James C. Patterson, Jr.  
NASA Langley Research Center

#### SUMMARY

Experimental wind-tunnel investigations have been conducted recently by the National Aeronautics and Space Administration to determine the aerodynamic interference associated with engine-pylon installations. The studies included the effects of powered jets. Tests were conducted on an aft-fuselage-mounted nacelle configuration over a Mach number range from 0.665 to 0.82 at Reynolds numbers of  $2.74 \times 10^6$  to  $3.94 \times 10^6$  based on the mean geometric chord of 3.2 inches. Tests were also conducted on a semispan model of a cargo-type logistic transport configuration with an underwing pylon-mounted powered-engine nacelle and on a 0.0576-scale semispan model of the Lockheed C-5A transport configuration. The effects of powered fan-jet model engines were included. These tests were conducted over a Mach number range from 0.70 to 0.825 at Reynolds numbers of  $6.10 \times 10^6$  to  $7.13 \times 10^6$  based on the mean geometric chord of 21.158 inches.

The results of these investigations indicate that favorable interference drag may be obtained by detailed tailoring of the engine nacelles and pylons to the airplane itself. The effect of the powered jet on aerodynamic interference is such that the favorable interference noted at the cruise Mach number was doubled throughout the higher lift-coefficient range of this investigation.

#### INTRODUCTION

One important fact to be considered in the design of airplanes of today is aerodynamic interference. Investigations to determine aerodynamic interference resulting from engine-pylon installations have been conducted recently by the NASA on a small transport configuration having aft-fuselage-mounted nacelles and on the more familiar underwing pylon-mounted nacelle configurations. The studies of the underwing configurations included the effects of a powered model of a fan-jet engine.

The ability to simulate the full-scale engine and nacelle aerodynamic and geometric effects in the wind tunnel is unique and offers the potential of obtaining engine-jet-stream interference effects which could very possibly result in new engine-installation methods.

## SYMBOLS

|                |   |
|----------------|---|
| $C_D$          | drag coefficient, Drag/qS   |
| $\Delta C_D$   | interference drag coefficient   |
| $C_L$          | lift coefficient  |
| $\Delta C_p$   | incremental pressure coefficient  |
| M              | Mach number   |
| $P_{t,e}$      | engine fan exit total pressure  |
| $P_{t,\infty}$ | free-stream total pressure  |
| q              | free-stream dynamic pressure  |
| $R_c$          | Reynolds number based on mean geometric chord   |
| S              | wing area   |
| $x/l$          | ratio of longitudinal distance from powered-engine leading edge to total length of powered engine |

## DISCUSSION

### Aft-Fuselage-Mounted Nacelle Configuration

A sting-supported model of a small transport configuration with engine nacelles pylon-mounted on the rear of the fuselage is shown in figure 1. Tests were conducted on this configuration with the engine nacelles mounted in various longitudinal locations, with the engine-nacelle incidence angle and cant angle varied to align the engines with the local flow, and with the pylons and engine nacelles extended chordwise (as shown by the dashed nacelle-pylon outline in fig. 1) in an attempt to improve the area distribution in the vicinity of the engine nacelles. The test Mach number ranged from 0.665 to 0.82.

The results of this investigation are presented as interference drag coefficient  $\Delta C_D$  for the various configurations tested. These interference-drag values are obtained from the difference between the drag level of the basic airplane configuration and that of the basic configuration less pylons and engine nacelles plus the calculated skin-friction drag of the pylons and engine nacelles throughout the Mach number range for a lift coefficient of 0.25. (See fig. 2.)

The interference-drag results obtained for the four previously mentioned configurations tested - engine longitudinal location, nacelle incidence angle,

cant angle, and engine and pylon extension - are shown in figure 3. The interference-drag results of the basic configuration are shown in each of the four plots for reference. The negative values of  $\Delta C_D$  represent favorable interference whereas the positive values represent interference drag. The results obtained for the basic configuration indicate interference drag in the lower Mach number range and favorable interference above a Mach number of 0.79.

The optimum longitudinal nacelle location, determined from tests conducted on a series of chordwise nacelle locations, was obtained by moving the nacelle-pylon combination rearward 27 percent of the wing mean aerodynamic chord from its original position on the basic configuration. The interference-drag results obtained for the improved longitudinal location indicate a reduction in interference drag coefficients over that obtained for the original location throughout the Mach number range with an increase in the favorable interference at the higher test Mach numbers.

To aline the engine nacelles with the local flow, tests were conducted through a nacelle-incidence-angle range from approximately  $0^\circ$  to  $4^\circ$ . The lowest interference drag results were obtained at an incidence angle of  $2.5^\circ$ . The effect of this incidence angle is shown in the lower left-hand plot of figure 3; throughout the Mach number range, the interference drag coefficient is reduced.

A cant angle of  $3.5^\circ$  was investigated (nacelle inlet directed outward), which resulted in a slight decrease in drag in the lower Mach number range, followed by a reduction in the favorable interference at higher Mach numbers. Since only one cant angle was investigated, it is possible that further improvement may very well be obtained at other cant angles.

The rearward chordwise engine nacelle and pylon extension, of approximately 25 percent of the nacelle length, increases the favorable interference from a Mach number of 0.775 to a Mach number of 0.82 as a result of an improvement in the local area distribution.

Unfortunately, tests were not conducted with the nacelle-pylon configuration in its most favorable location, but the configuration changes investigated are such that their contributions to interference drag may very possibly be additive. Nevertheless, the data presented indicate that the aerodynamic interference can be reduced and a favorable interference produced in many cases as a result of tailoring the nacelle-pylon combination to the airplane itself by taking into consideration the area distributions and local flow conditions.

#### Underwing Pylon-Mounted Engine Nacelles Including Power Effect

Investigations including the effects of the fan-jet flow on the aerodynamic interference have also been made of the more familiar underwing pylon-mounted engine configuration. With the development of the current high-bypass fan-jet engines, the exact effect that the fan-jet flow has on aerodynamic interference has become very important. An investigation to determine this power

effect has recently been conducted with the use of a semispan model of a cargo type airplane configuration. Figure 4 shows this model installed in the Langley 8-foot transonic pressure tunnel. The fuselage is mounted directly on the tunnel wall while the wing is mounted directly on the force balance. A powered model of a fan-jet engine is pylon-mounted under the wing. The force results were obtained for the wing-pylon-engine combination and included the influence of the presence of the fuselage on these components.

The interference drag coefficient  $\Delta C_D$  for the powered-model test was obtained by reducing the total drag measured with the force balance by the computed thrust and by the drag of the three individual components of the model: wing, engine, and pylon. This procedure is shown by the following equation:

$$\Delta C_D = (C_D)_{\text{total}} + C_F - (C_D)_{\text{wing}} - (C_D)_{\text{engine}} - (C_{D,f})_{\text{pylon}}$$

where

- $(C_D)_{\text{total}}$  total measured wing-pylon-engine drag coefficient, obtained from wall-mounted strain-gage force balance
- $C_F$  engine net thrust coefficient based on wing area, computed from total-pressure and static-pressure measurements taken in fan inlet, fan exit, turbine inlet, and turbine exit
- $(C_D)_{\text{wing}}$  wing-drag coefficient, obtained from wall-mounted strain-gage force balance during tests made with the engine and pylon removed
- $(C_D)_{\text{engine}}$  measured drag coefficient less pylon drag coefficient and less engine net thrust coefficient for the engine alone
- $(C_{D,f})_{\text{pylon}}$  pylon skin-friction drag coefficient, calculated by using skin-friction values from the Sommer and Short 'T' method (see ref. 1)

The engine-alone measurements were obtained during tests of the engine mounted on an elongated pylon that was mounted directly on the balance. The pylon drag was measured during tests performed with the engine removed from this configuration. The engine net thrust was obtained from the same type of pressure measurements and computing method used during the complete-configuration test.

Fan-jet engine.— The general outline of the full-scale fan-jet engine which is to be used on the C-5A logistic transport is shown in figure 5. The engine is approximately 25 feet long and has a maximum fan-cowl diameter of 9 feet. Eighty-five percent of the maximum thrust of 41 000 pounds is produced by this fan. With a bypass ratio of 8.1, approximately 1335 lb/sec of the total engine weight flow of 1500 lb/sec passes through the fan, whereas 165 lb/sec of air enters the primary discharge nozzle.

An effort was made during the design of this engine to maintain an area distribution which would be compatible to that of the overall area buildup of the C-5A type airplane configuration. This effort has resulted in a smooth total area distribution for the engine-airplane combination.

Model engine.- A cross-sectional view of the powered model of the C-5A engine used during this investigation is shown in figure 6. The two-stage fan is connected directly to the nitrogen-driven three-stage turbine. This model engine was designed to produce the same mass-flow ratio and exit-pressure ratio as the actual full-scale engine. At the maximum design speed of 45 000 rpm, the model engine, which has a maximum diameter of 5.9 inches and an overall length of 18 inches, develops approximately 130 horsepower.

Total-pressure rakes and static-pressure taps were located in the fan inlet, in the fan exit, and in the turbine exit to obtain the measurements to be used in computing thrust. A total of 276 pressures were recorded during this investigation and included surface pressures on the fan cowl, turbine, turbine exit plug, pylon surfaces, and wing upper and lower surfaces in the vicinity of the wing-pylon juncture.

Jet effects.- The effect of the powered fan-jet engine on the aerodynamic interference is shown in figure 7 as the interference drag coefficient  $\Delta C_D$  plotted against lift coefficient for fan-exit pressure ratios of 1.0 and 1.47. A pressure ratio of 1.0 is obtained with the engine operating just fast enough to overcome the internal losses of the engine, and zero thrust is produced. A pressure ratio of 1.47 is obtained for the maximum design speed, where maximum thrust is produced. The data indicate that with power on, the favorable interference is increased throughout the lift-coefficient range, with a maximum increase of approximately 10 drag counts at the highest lift coefficient.

A possible explanation for the increase in favorable interference may be that with the engine operating at the zero thrust condition, there is a tendency for the pressure to become equalized on the inboard and outboard sides of the pylon. This balance of pylon pressure is believed to be caused by a pressure leakage that takes place between the fan cowl and the turbine cowl, as shown by the arrow in the cutaway oblique view of the engine in figure 7. The change in pressure coefficient ( $\Delta C_p$ ) between the inboard side and the outboard side of the pylon measured along the nacelle-pylon juncture is presented in the lower plot of figure 7 as a function of nacelle length.

The pressure difference is small for the zero thrust condition; however, with the engine producing maximum thrust, the fan exit is choked and the pressure leakage from the inboard side to the outboard side of the pylon cannot occur. This is shown in figure 7 as an increase in the difference in pressure coefficient. This increase in pylon normal force is believed to be a result of an increase in the end-plate effectiveness of the engine nacelle with the fan exit choked plus the effect of the increase in the fan-jet flow over the rear portion of the pylon. This pylon normal force, when reduced to a lift vector perpendicular to the local flow, results in a thrust vector in the stream direction, because of the direction of this local flow associated with the

swept wing. This induced thrust may possibly account, in part, for the favorable interference obtained with power on.

C-5A logistics transport.- Further investigations have been made by using a semispan model of the C-5A logistics transport configuration mounted in the Langley 8-foot transonic pressure tunnel. Again, the fuselage was mounted directly on the tunnel wall and the wing was mounted directly on the force balance. Two powered fan-jet engines were pylon-mounted under the wing of the C-5A model as shown in figure 8. A total of 552 surface pressures and total rake pressures were measured during this two-engine investigation.

Engine position.- The results obtained from an investigation of engine position are shown as interference drag plotted against Mach number in figure 9 for the basic engine position, for the engine moved rearward, and for the engine moved rearward and vertically upward. The data indicate that the greatest favorable interference effect is obtained with the engine in the most forward position. These results substantiate results obtained previously (not shown herein) for the one-engine test where it was also found that with the engine in the foremost longitudinal and lowest vertical position the most favorable interference results were obtained.

The data in figure 9 indicate that interference drag is very sensitive to engine position. With the engine moved rearward approximately 10 percent of the engine length, favorable interference is obtained in the lower Mach range; before the cruise Mach number is reached, however, the interference drag coefficient becomes unfavorable. The reduction in pylon leading-edge sweep associated with this rearward movement of the engine from  $77.5^\circ$  to  $74^\circ$  results in an increase in pylon side force which may possibly account for the favorable interference obtained for this configuration at the lower Mach numbers. The unfavorable interference drag obtained in the higher Mach number range would result from the change in the area distribution caused by this change in engine position. As the engine is moved closer to the wing, the interference drag is increased even further and, in fact, no favorable effects occur throughout the Mach number range. These results, in the lower Mach number range, may be attributed to the increase in pylon leading-edge sweep and the associated loss in side force; in the higher Mach number range, they may be attributed to a magnification of the already unfavorable effects associated with the change in area distribution as the engine is moved even closer to the wing.

Pylon leading-edge extension.- The effect of pylon leading-edge extension was also investigated. Figure 10 shows the two pylon configurations tested. The first pylon has a leading edge sweep of  $74^\circ$  and is attached to the lower surface of the wing, just behind the wing leading edge, as proposed for the C-5A airplane. The second pylon, having the same sweep, has its leading edge extended forward approximately 10 percent of the pylon chord. This extension results in the pylon leading edge extending over the wing, as shown by the dashed outline on the sketch in the upper part of the figure.

The data indicate that the configuration having the originally proposed pylon configuration provided favorable interference at the cruise Mach number. The extended-eylon configuration produced approximately zero interference drag

in the lower Mach number range, becoming unfavorable at the higher test Mach numbers. Further wind-tunnel investigations will be necessary before an explanation can be given for this difference in interference drag resulting from this change in pylon extension.

### CONCLUSIONS

Wind-tunnel studies of nacelle interference drag at high subsonic speeds including the effect of powered jets have been presented. The data indicate that the aerodynamic interference resulting from nacelle-ptylon installation may be minimized or even made favorable by properly locating the engine nacelles and by detailed tailoring of the engine-ptylon configuration. It has also been shown that the effect of the powered jet is such that the favorable interference noted in this investigation was doubled throughout the higher lift-coefficient range. Inasmuch as only a few possible engine installations have been studied herein, it should be emphasized that more extensive wind-tunnel investigations will be required before the exact effect that the powered jets have on interference drag can be fully understood.

### REFERENCE

1. Peterson, John B., Jr.: A Comparison of Experimental and Theoretical Results for the Compressible Turbulent-Boundary-Layer Skin Friction With Zero Pressure Gradient. NASA TN D-1795, 1963.

AFT-FUSELAGE-MOUNTED NACELLES  
 WING AREA, 51.5 SQ IN.; MEAN AERODYNAMIC CHORD, 3.2 IN.;  
 $R_{\xi} = 2.74$  TO  $3.94 \times 10^6$

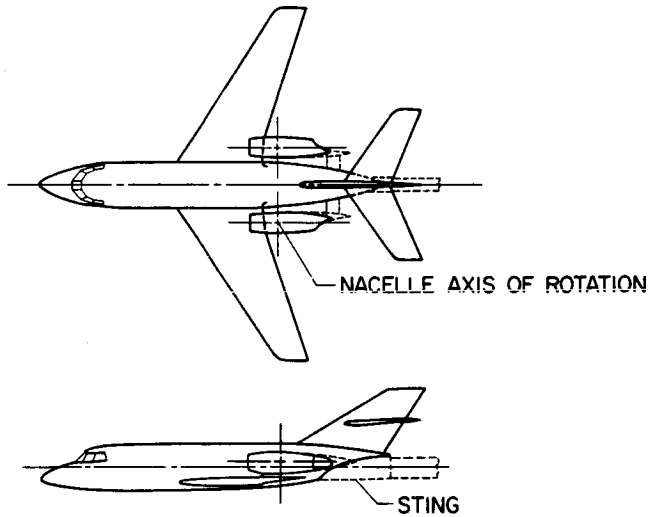


Figure 1

ENGINE NACELLE-PYLON DRAG  
 $C_L = 0.25$

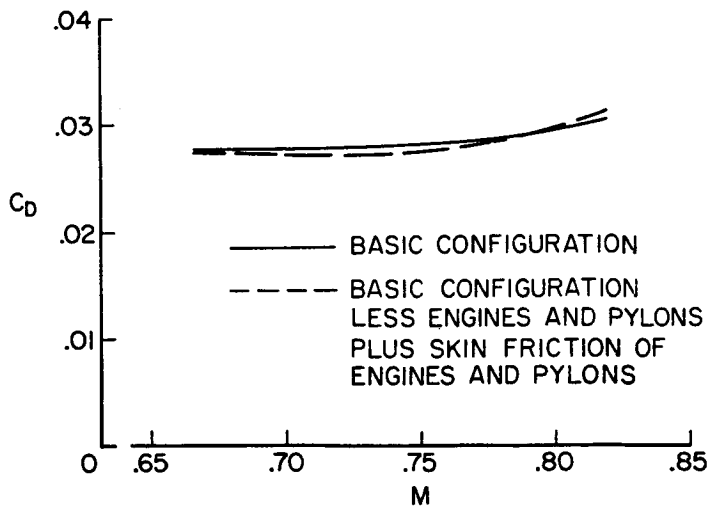


Figure 2

# INTERFERENCE DRAG

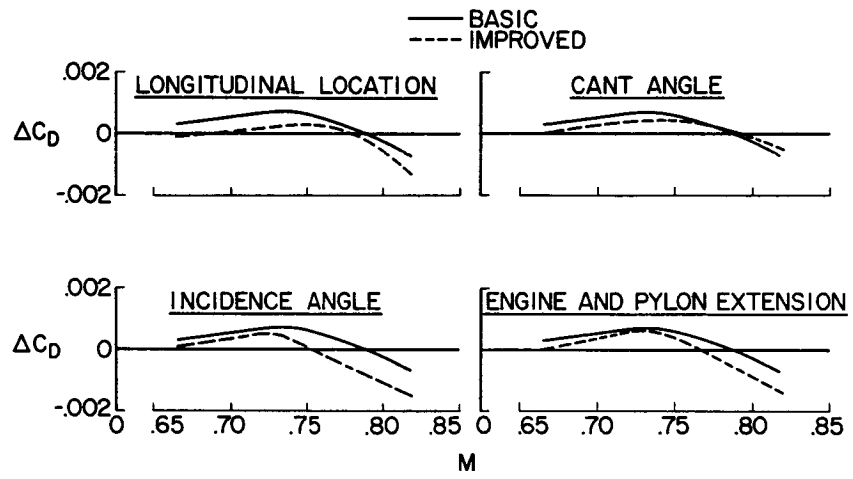


Figure 3

## CARGO-TYPE AIRPLANE MODEL WITH POWERED ENGINE

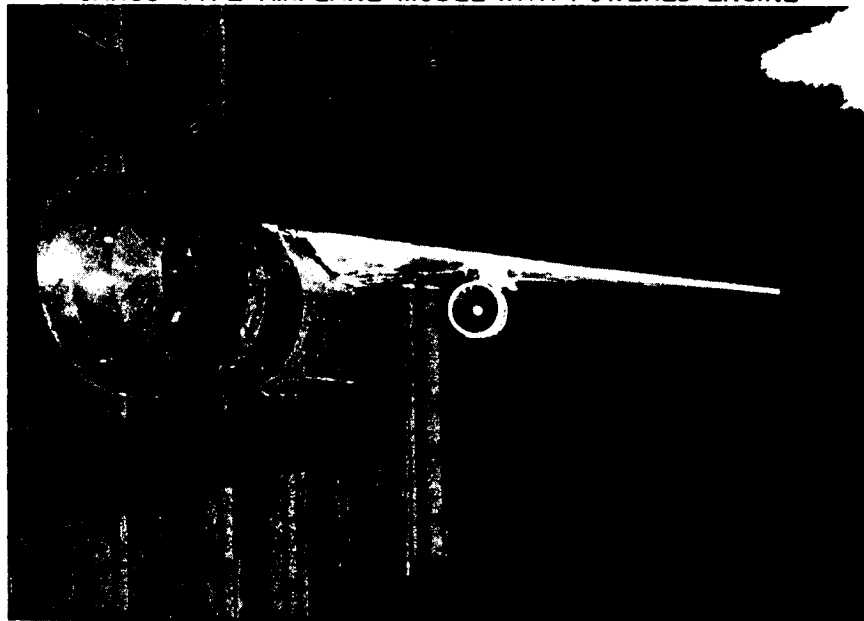


Figure 4

L-2683-6

CONFIGURATION OF C-5A FAN-JET ENGINE

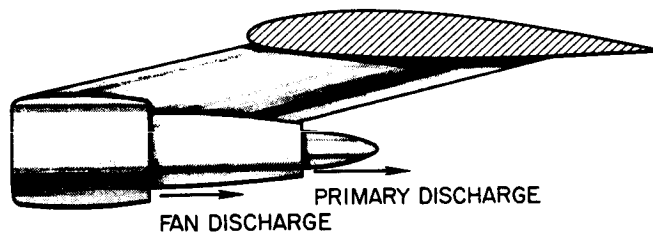


Figure 5

MODEL-ENGINE CROSS SECTION

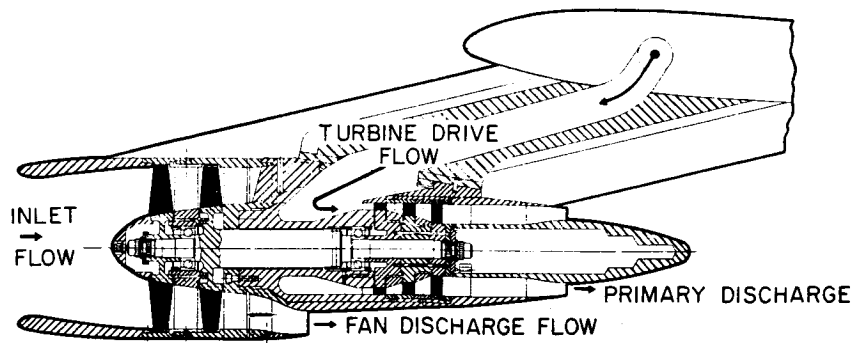


Figure 6

ENGINE-JET EFFECT  
M=0.78

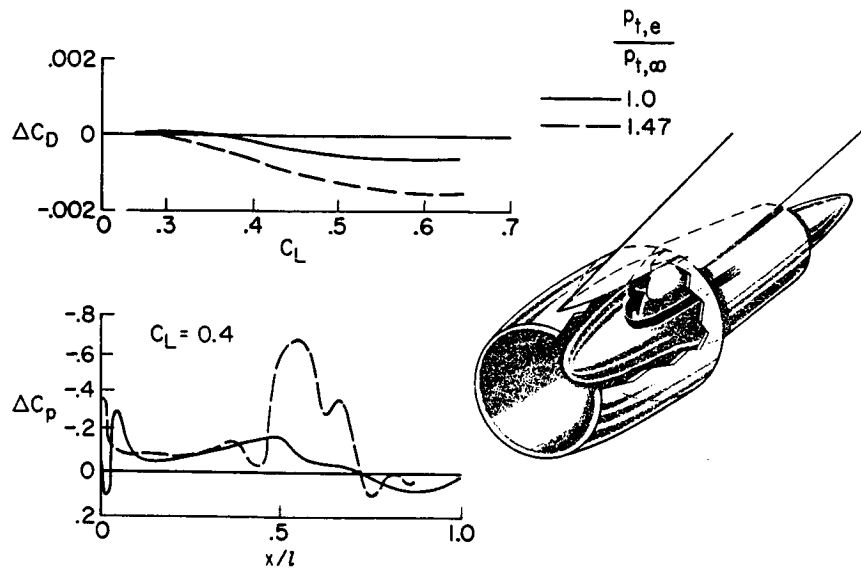


Figure 7

C-5A MODEL WITH POWERED ENGINES

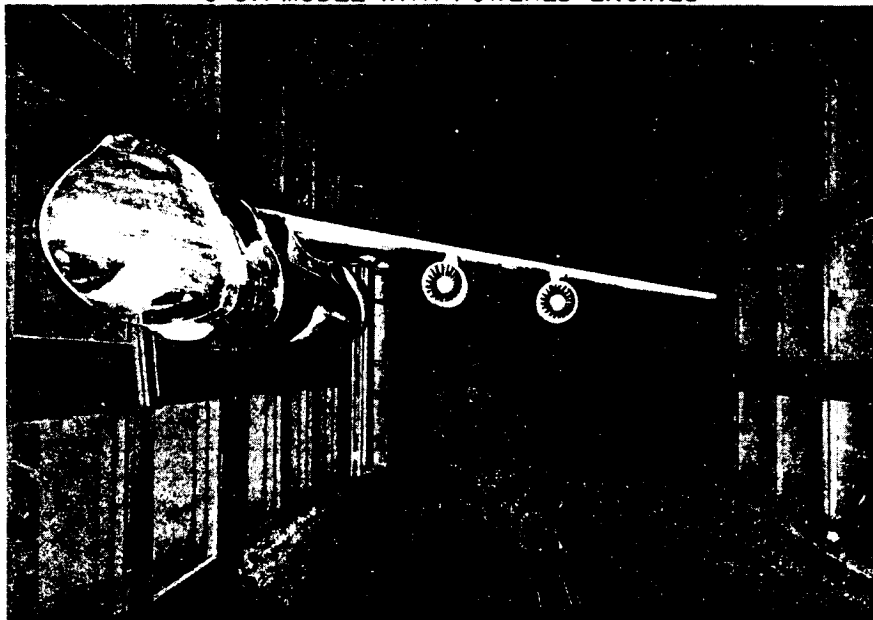


Figure 8

L-2683-5

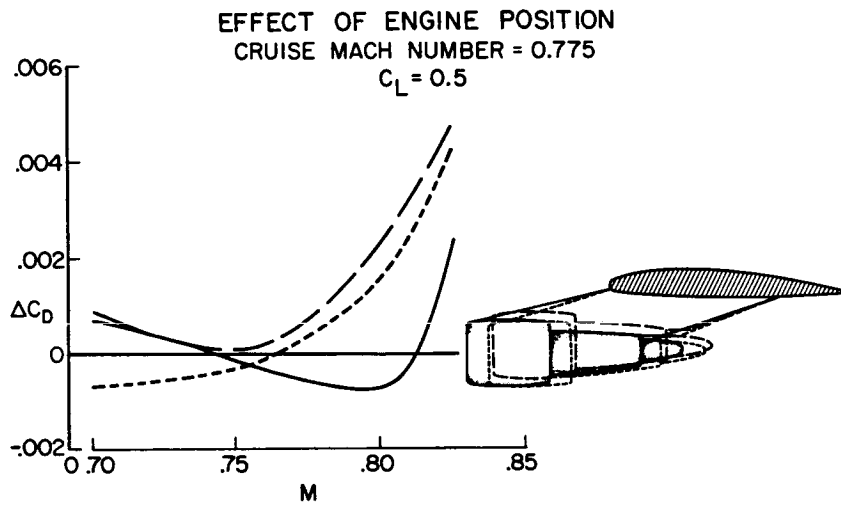


Figure 9

**EFFECT OF PYLON LEADING-EDGE EXTENSION**  
**CRUISE MACH NUMBER = 0.775**  
 $C_L = 0.5$

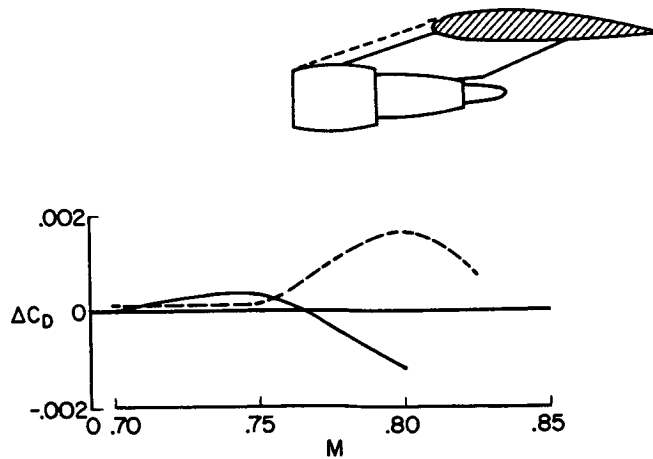


Figure 10